



The Broad-lined Ic Supernova ZTF18aaqjovh (SN 2018bvw): An Optically Discovered Engine-driven Supernova Candidate with Luminous Radio Emission

Anna Y. Q. Ho¹ , Alessandra Corsi² , S. Bradley Cenko^{3,4} , Francesco Taddia⁵, S. R. Kulkarni¹ , Scott Adams¹, Kishalay De¹, Richard Dekany⁶, Dmitry D. Frederiks⁷ , Christoffer Fremling¹ , V. Zach Golkhou^{8,9,18} , Matthew J. Graham¹ , Tiara Hung¹⁰ , Thomas Kupfer¹¹ , Russ R. Laher¹² , Ashish Mahabal^{1,13}, Frank J. Masci¹² , Adam A. Miller^{14,15} , James D. Neill⁶ , Daniel Reiley⁶, Reed Riddle⁶ , Anna Ridnaia⁷, Ben Rusholme¹² , Yashvi Sharma¹, Jesper Sollerman⁵ , Maayane T. Soumagnac^{16,17} , Dmitry S. Svinkin⁷ , and David L. Shupe¹² 

¹ Cahill Center for Astrophysics, California Institute of Technology, MC 249-17, 1200 E California Boulevard, Pasadena, CA, 91125, USA; ah@astro.caltech.edu

² Department of Physics and Astronomy, Texas Tech University, Box 1051, Lubbock, TX 79409-1051, USA

³ Astrophysics Science Division, NASA Goddard Space Flight Center, Mail Code 661, Greenbelt, MD 20771, USA

⁴ Joint Space-Science Institute, University of Maryland, College Park, MD 20742, USA

⁵ Department of Astronomy, The Oskar Klein Center, Stockholm University, AlbaNova, SE-10691 Stockholm, Sweden

⁶ Caltech Optical Observatories, California Institute of Technology, Pasadena, CA, USA

⁷ Ioffe Institute, Politekhnicheskaya 26, St. Petersburg 194021, Russia

⁸ DIRAC Institute, Department of Astronomy, University of Washington, 3910 15th Avenue NE, Seattle, WA 98195, USA

⁹ The eScience Institute, University of Washington, Seattle, WA 98195, USA

¹⁰ Department of Astronomy and Astrophysics, University of California, Santa Cruz, CA 95064, USA

¹¹ Kavli Institute for Theoretical Physics, University of California, Santa Barbara, CA 93106, USA

¹² IPAC, California Institute of Technology, 1200 E. California Boulevard, Pasadena, CA 91125, USA

¹³ Center for Data Driven Discovery, California Institute of Technology, Pasadena, CA 91125, USA

¹⁴ Center for Interdisciplinary Exploration and Research in Astrophysics (CIERA) and Department of Physics and Astronomy, Northwestern University, 2145 Sheridan Road, Evanston, IL 60208, USA

¹⁵ The Adler Planetarium, Chicago, IL 60605, USA

¹⁶ Lawrence Berkeley National Laboratory, 1 Cyclotron Road, Berkeley, CA 94720, USA

¹⁷ Department of Particle Physics and Astrophysics, Weizmann Institute of Science, Rehovot 76100, Israel

Received 2019 December 20; revised 2020 February 25; accepted 2020 March 2; published 2020 April 23

Abstract

We present ZTF18aaqjovh (SN 2018bvw), a high-velocity (“broad-lined”) stripped-envelope (Type Ic) supernova (Ic-BL SN) discovered in the Zwicky Transient Facility one-day cadence survey. ZTF18aaqjovh shares a number of features in common with engine-driven explosions: the photospheric velocity and the shape of the optical light curve are very similar to those of the Type Ic-BL SN 1998bw, which was associated with a low-luminosity gamma-ray burst (LLGRB) and had relativistic ejecta. However, the radio luminosity of ZTF18aaqjovh is almost two orders of magnitude fainter than that of SN 1998bw at the same velocity phase, and the shock velocity is at most mildly relativistic ($v = 0.06\text{--}0.4c$). A search of high-energy catalogs reveals no compelling gamma-ray burst (GRB) counterpart to ZTF18aaqjovh, and the limit on the prompt GRB luminosity of $L_{\gamma,\text{iso}} \approx 1.6 \times 10^{48} \text{ erg s}^{-1}$ excludes a classical GRB but not an LLGRB. Altogether, ZTF18aaqjovh represents another transition event between engine-driven SNe associated with GRBs and “ordinary” Ic-BL SNe.

Unified Astronomy Thesaurus concepts: Core-collapse supernovae (304); Type Ic supernovae (1730); Supernovae (1668); Hypernovae (775); Radio transient sources (2008); Transient sources (1851); High energy astrophysics (739); Time domain astronomy (2109); Sky surveys (1464)

Supporting material: data behind figure

1. Introduction

Broad-lined Type Ic supernovae (Ic-BL SNe) are a subclass of stripped-envelope core-collapse supernovae (CC SNe) characterized by fast ejecta and large kinetic energies. While typical Type Ic SNe have photospheric velocities $v_{\text{ph}} \approx 10,000 \text{ km s}^{-1}$ (measured from Fe II absorption features), Type Ic-BL SNe have $v_{\text{ph}} \approx 20,000 \text{ km s}^{-1}$ at maximum light (Modjaz et al. 2016). The kinetic energy release of Ic-BL SNe is typically $\sim 10^{52} \text{ erg}$ (Cano 2013; Lyman et al. 2016; Prentice et al. 2016), an order of magnitude greater than traditional CC SNe (Woosley & Janka 2005), although this measurement is highly model-dependent.

A clue to the high energies and fast velocities present in Ic-BL SNe is their connection to long-duration gamma-ray

bursts, reviewed in Woosley & Bloom (2006), Hjorth & Bloom (2012), and Cano et al. (2017). The association began with the coincident discovery of GRB 980425 and SN 1998bw at $d = 40 \text{ Mpc}$ (Galama et al. 1998; Kulkarni et al. 1998). However, GRB 980425 was different from typical gamma-ray bursts (GRBs): it was underluminous in γ -rays ($L_{\gamma,\text{iso}} \sim 5 \times 10^{46} \text{ erg s}^{-1}$ compared to typical values of $10^{51}\text{--}10^{53} \text{ erg s}^{-1}$) and subenergetic, with an isotropic equivalent energy four orders of magnitude smaller than that of typical GRBs. Thus, it took the discovery of the cosmological GRB 030329 ($z = 0.1685$) in association with SN 2003dh (Hjorth et al. 2003; Stanek et al. 2003) to solidify the relationship between GRBs and SNe.

Since then, ~ 20 SNe accompanying GRBs have been spectroscopically confirmed. All show broad Type Ic-BL features near maximum light, with two exceptions: SN 2011kl had a relatively featureless spectrum, and SN 2013ez more

¹⁸ Moore-Sloan, WRF Innovation in Data Science, and DIRAC Fellow.

closely resembled a Type Ic (Cano et al. 2017). The GRB-SN association has led to the suggestion that GRBs and Ic-BL SNe are powered by a single central engine (Lazzati et al. 2012; Sobacchi et al. 2017; Barnes et al. 2018). However, a systematic search for radio emission from Ic-BL SNe constrained the fraction harboring a relativistic outflow as bright as that of SN 1998bw to be $\lesssim 14\%$ (Corsi et al. 2016).

Complicating matters, additional underluminous GRBs have been discovered since GRB 980425 and are collectively referred to as low-luminosity GRBs (LLGRBs). LLGRBs are distinguished by isotropic peak luminosities $L_{\text{iso}} \approx 10^{46}\text{--}10^{48} \text{ erg s}^{-1}$ and a relativistic energy release that is 2–3 orders of magnitude smaller than the 10^{51} erg from GRBs with fully relativistic outflows (Cano et al. 2017). Due to their lower intrinsic luminosities, LLGRBs are discovered at low redshifts ($z \lesssim 0.1$). Thus, despite the fact that their intrinsic rate might be 10–100 larger than that of classical GRBs (Soderberg et al. 2006; Pian et al. 2006), only seven have been discovered: LLGRB 980425/SN 1998bw, XRF 020903 (Sakamoto et al. 2004; Soderberg et al. 2004a; Bersier et al. 2006), LLGRB 031203/SN 2003lw (Malesani et al. 2004; Soderberg et al. 2004b; Thomsen et al. 2004; Watson et al. 2004), LLGRB 060218/SN 2006aj (Mirabal et al. 2006; Pian et al. 2006; Soderberg et al. 2006), LLGRB 100316D/SN 2010bh (Starling et al. 2011; Bufano et al. 2012), LLGRB 171205A/SN 2017iuk (D’Elia & Campana 2018; Wang et al. 2018), and most recently LLGRB 190829A (Chand et al. 2020). LLGRB 060218 and LLGRB 100316D have their own distinct properties: a long γ -ray prompt emission phase, and long-lived soft X-ray emission that might arise from continued activity of the central engine (Soderberg et al. 2006; Margutti et al. 2013) or dust echoes (Margutti et al. 2015; Irwin & Chevalier 2016).

Modeling of the radio emission from LLGRBs suggests quasi-spherical ejecta coupled to mildly relativistic material, with no off-axis components (Kulkarni et al. 1998; Soderberg et al. 2006; Pian et al. 2006; Margutti et al. 2013). Thus, it seems that LLGRBs arise from a fundamentally different mechanism to cosmological GRBs. One suggestion is that they represent failed or choked-jet events, and that the gamma-rays arise from shock breakout (Bromberg et al. 2011). This is supported by the early light curve of the LLGRB 060218, whose double peak in ultraviolet and optical filters has been modeled as shock breakout into a dense stellar wind (Campana et al. 2006) or into an extended envelope (Nakar 2015). Another suggestion is that they arise from a successful low-luminosity jet (Irwin & Chevalier 2016).

A major focus of scientific investigation over the past 20 years has been to unify this diverse array of phenomena: “extreme” SNe with successful, observed jets (classical GRBs), mildly relativistic explosions (LLGRBs or radio-emitting SNe), and ordinary (nonrelativistic) SNe. The traditional avenue to discovering central engines—the detection of a GRB—is severely limited because a number of conditions must be met for a central engine to produce a GRB. First, the jet must be nearly baryon-free—else the available energy is insufficient to accelerate the ejecta to ultrarelativistic velocities, and gamma-ray emission will be stifled by pair-production (Piran 2004). Next, the jet must successfully escape the star without being choked by the stellar envelope (MacFadyen et al. 2001). Finally, the jet must be directed at Earth.

Today, wide-field optical time-domain surveys have the field of view and cadence to discover engine-driven explosions

without relying on a high-energy trigger (e.g., Corsi et al. 2017). Radio observations are central to this effort, because they trace the fastest-moving ejecta. The Zwicky Transient Facility (ZTF; Bellm et al. 2019b; Graham et al. 2019) is conducting several different surveys (Bellm et al. 2019a) using a custom mosaic camera (Dekany et al. 2016) on the 48 inch Samuel Oschin Telescope (P48) at the Palomar Observatory. ZTF discovers one Ic-BL SN per month, and we are conducting a follow-up campaign of a subset of these events with the Karl G. Jansky Very Large Array (VLA; Perley et al. 2011). Here, we present our first detection of radio emission from the Ic-BL ZTF18aaqjovh (SN 2018bvw). In Section 2 we describe our optical, radio, and X-ray observations, as well as our search for contemporaneous gamma-ray emission. In Section 3 we constrain the physical properties of the explosion (energy, velocity, and ejecta mass). We present our conclusions in Section 4.

Throughout the paper we use the Λ CDM cosmology from Planck Collaboration et al. (2016).

2. Observations

2.1. Zwicky Transient Facility Discovery

ZTF images are processed and reference-subtracted by the IPAC ZTF pipeline (Masci et al. 2019) using the method described in Zackay et al. (2016), and every 5σ point-source detection is saved as an “alert.” Alerts are distributed in Apache Avro format (Patterson et al. 2019) and can be filtered based on a machine-learning real-bogus metric (Duev et al. 2019; Mahabal et al. 2019), host characteristics (including a star-galaxy classifier; Tachibana & Miller 2018¹⁹), and light-curve properties. The ZTF collaboration uses a web-based system called the GROWTH marshal (Kasliwal et al. 2019) to identify, monitor, and coordinate follow-up observations for transients of interest.

ZTF18aaqjovh was discovered in an image obtained on 2018 May 5 UT as part of the ZTF one-day cadence survey, which covers 3000 deg^2 in two visits (one g , one r) per night (Bellm et al. 2019a). The alert passed two filters, as part of two systematic surveys being conducted by ZTF: a filter for transients in the local universe that cross-matches sources with a catalog of nearby galaxies (Cook et al. 2019), and a filter for bright transients (Fremling et al. 2019c). Because it passed these filters, the source was reported to the Transient Name Server (TNS²⁰; Fremling & Taggart 2018) and received the designation SN 2018bvw. After being reported, it was spectroscopically classified (Section 2.2; Fremling et al. 2019a).

The discovery magnitude was $r = 18.65 \pm 0.02 \text{ mag}$, where the error bar is a 1σ estimate of the background rms, derived using a pixel-uncertainty map created for the difference image (Masci et al. 2019). The source position was measured to be $\alpha = 1^{\text{h}}52^{\text{m}}43^{\text{s}}.62$, $\delta = +25^{\text{d}}40^{\text{m}}30^{\text{s}}.1$ (J2000). The position is $4''.71$ from SDSS J115244.11+254027.1, a star-forming galaxy at $z = 0.05403 \pm 0.00001$ (248.85 Mpc; Alam et al. 2015). The transient position with respect to the host galaxy is shown in Figure 1, with the host galaxy image constructed from SDSS g -, r -, and i -band cutouts using the method in Lupton et al. (2004). At this distance, the projected offset between ZTF18aaqjovh and the center of the host corresponds to $d = 5.68 \text{ kpc}$. This offset is larger than the typical offset of Ic-BL SNe accompanied by GRBs, which is $1.54_{-1.28}^{+3.13} \text{ kpc}$

¹⁹ In this context TM18 define star as an unresolved point source and galaxy as an extended unresolved source.

²⁰ <https://wis-tns.weizmann.ac.il>

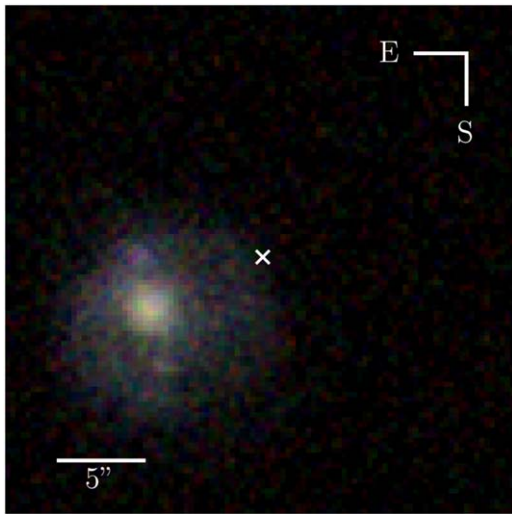


Figure 1. Image of the host galaxy of ZTF18aaqjovh (SN 2018bvw), constructed from g -, r -, and i -band SDSS cutouts. The position of ZTF18aaqjovh is shown with a white cross, $4''.71$ from the center of the galaxy, or 5.68 kpc assuming $d = 249$ Mpc.

(1σ confidence), and more consistent with the offsets of Ic-BL SNe without detected GRBs, measured to be $(3.08_{-2.35}^{+2.98})$ kpc (Japelj et al. 2018).

The full light curve, corrected for Milky Way extinction, is provided in Table 1 and shown in Figure 2. The P48 measurements come from forced photometry (Yao et al. 2019). The g -band reference image was constructed from data taken between 2018 April 22 and 2018 May 16, so we had to subtract a baseline flux to account for SN light in the reference. To calculate the baseline flux, we measured the mean flux of photometry in images where the SN light was not present: a set of images at $\Delta t \approx -50$ days and a set of images at $\Delta t \approx 400$ days. We confirmed that this baseline level was consistent, i.e., that by 400 days the SN light had returned to a level consistent with the pre-explosion level.

We obtained two epochs of photometry from the Spectral Energy Distribution Machine (SEDM; Blagorodnova et al. 2018; Rigault et al. 2019) mounted on the automated 60 inch telescope at Palomar (P60; Cenko et al. 2006). Digital image subtraction and photometry for the SEDM was performed using the Fremling Automated Pipeline (FPipe; Fremling et al. 2016). Fpipe performs calibration and host subtraction against SDSS reference images and catalogs (Ahn et al. 2014).

The peak r -band absolute magnitude is typical of Ic-BL light curves compiled from untargeted surveys (Taddia et al. 2019), and the light curve of ZTF18aaqjovh is very similar in shape to the light curve of SN 1998bw (Figure 2). Assuming that the time from explosion to peak is the same in ZTF18aaqjovh as in SN 1998bw, we can estimate that the explosion time t_0 is about the time of the last nondetection, 2018 April 25 UT. The optical spectra of ZTF18aaqjovh (Section 2.2) suggest that this t_0 is accurate to within a few days: the spectrum of ZTF18aaqjovh on May 9 was most similar to that of SN 1998bw at 16 days post-explosion. With this t_0 , the first detection of ZTF18aaqjovh by ZTF was at $\Delta t = 10$ days. Throughout the paper, we use this definition of t_0 and report all times Δt with respect to this reference point.

Table 1
Optical Light Curve of ZTF18aaqjovh from Forced Photometry on P48 Images (Yao et al. 2019)

Date (MJD)	Δt	Instrument	Filter	AB Mag	Error in AB Mag
58243.170324	9.99	P48	r	18.59	0.03
58244.170880	10.99	P48	r	18.47	0.02
58245.171447	12.00	P48	r	18.32	0.02
58245.172384	12.00	P48	r	18.31	0.02
58246.233762	13.06	P48	r	18.32	0.03
58247.234363	14.06	P48	r	18.28	0.02
58247.358800	14.18	P60	r	18.30	0.04
58248.235324	15.06	P48	r	18.21	0.02
58248.236250	15.06	P48	r	18.17	0.02
58248.335300	15.16	P60	r	18.21	0.03
58249.234444	16.06	P48	r	18.23	0.03
58250.234803	17.06	P48	r	18.17	0.03
58254.191401	21.02	P48	r	18.31	0.02
58254.192338	21.02	P48	r	18.26	0.02
58255.238356	22.06	P48	r	18.32	0.02
58256.217651	23.04	P48	g	19.02	0.05
58256.218113	23.04	P48	g	18.98	0.05
58256.218565	23.04	P48	g	19.06	0.06
58256.219028	23.04	P48	g	19.05	0.05
58256.219479	23.04	P48	g	19.05	0.04
58256.219942	23.04	P48	g	19.02	0.03
58256.220393	23.04	P48	g	19.03	0.02
58256.220845	23.04	P48	g	19.07	0.03
58256.221308	23.05	P48	g	19.11	0.02
58256.221759	23.05	P48	g	19.05	0.02
58256.222222	23.05	P48	g	19.04	0.03
58256.222674	23.05	P48	g	19.04	0.03
58256.223125	23.05	P48	g	19.04	0.03
58256.223588	23.05	P48	g	19.12	0.03
58256.244317	23.07	P48	r	18.40	0.03
58256.278032	23.10	P48	r	18.43	0.02
58257.232951	24.06	P48	r	18.42	0.03
58257.233877	24.06	P48	r	18.41	0.03
58258.168634	24.99	P48	g	19.32	0.04
58262.202593	29.03	P48	r	18.72	0.04
58262.220127	29.04	P48	g	19.53	0.08
58262.252870	29.08	P48	r	18.64	0.05
58263.235185	30.06	P48	r	18.74	0.03
58263.259248	30.08	P48	g	19.81	0.11
58266.250648	33.07	P48	r	19.02	0.07
58266.251562	33.08	P48	r	19.08	0.07
58267.185671	34.01	P48	g	20.08	0.29
58267.290174	34.11	P48	r	18.91	0.07
58268.167917	34.99	P48	g	20.13	0.24
58269.185035	36.01	P48	r	19.20	0.07
58269.185972	36.01	P48	r	19.08	0.06
58270.173681	37.00	P48	r	19.28	0.05
58272.184954	39.01	P48	r	19.37	0.04
58272.185880	39.01	P48	r	19.26	0.04
58274.198912	41.02	P48	r	19.45	0.05
58276.198576	43.02	P48	r	19.67	0.05
58276.199502	43.02	P48	r	19.50	0.05
58276.213970	43.04	P48	g	20.51	0.11
58276.214907	43.04	P48	g	20.56	0.11
58277.193495	44.02	P48	g	20.75	0.15
58277.243113	44.07	P48	r	19.51	0.06
58278.194016	45.02	P48	g	20.32	0.13
58278.237199	45.06	P48	r	19.62	0.07
58279.171516	46.00	P48	r	19.63	0.08
58279.187500	46.01	P48	r	19.63	0.06
58279.207593	46.03	P48	g	20.63	0.13
58279.208530	46.03	P48	g	20.60	0.12

Table 1
(Continued)

Date (MJD)	Δt	Instrument	Filter	AB Mag	Error in AB Mag
58280.174988	47.00	P48	<i>r</i>	19.63	0.09
58280.227755	47.05	P48	<i>g</i>	20.85	0.15
58281.194468	48.02	P48	<i>r</i>	19.76	0.07
58281.237141	48.06	P48	<i>g</i>	20.65	0.14
58282.193773	49.02	P48	<i>r</i>	19.77	0.07
58282.194699	49.02	P48	<i>r</i>	19.82	0.07
58282.243113	49.07	P48	<i>g</i>	20.51	0.14
58282.244039	49.07	P48	<i>g</i>	20.58	0.15
58283.215544	50.04	P48	<i>r</i>	19.81	0.07
58283.237836	50.06	P48	<i>g</i>	20.45	0.13
58284.203982	51.03	P48	<i>r</i>	19.80	0.08
58284.214236	51.04	P48	<i>g</i>	20.83	0.17

Note. Values have been corrected for Milky Way extinction. Phase is relative to t_0 defined in Section 2.1.

2.2. Spectral Classification

A log of our spectroscopic follow-up observations of ZTF18aaqjovh is provided in Table 2.

On 2018 May 9 UT we obtained a spectrum of ZTF18aaqjovh using the SEDM and compared it to a set of spectral templates from the publicly available Supernova Identification code (SNID; Blondin & Tonry 2007). The best match was to a spectrum of SN 1998bw taken at 16 days post-explosion. As shown in Figure 2, a comparison with the light curve of SN 1998bw suggests that these two spectra were obtained at comparable phases. So, we classified ZTF18aaqjovh as Type Ic-BL.

On 2018 May 14 UT, we observed ZTF18aaqjovh using the Low Resolution Imaging Spectrometer (Oke et al. 1995) on the Keck I 10 m telescope. The spectrum was reduced and extracted using LPipe (Perley 2019). The next day, we observed the source using the Andalusia Faint Object Spectrograph and Camera (ALFOSC²¹) on the Nordic Optical Telescope (NOT; Djupvik & Andersen 2010). The NOT spectrum was reduced in a standard way, including wavelength calibration against an arc lamp, and flux calibration using a spectrophotometric standard star. We obtained another spectrum on 2018 June 8 UT using the Double Beam Spectrograph (DBSP; Oke & Gunn 1982) on the 200 inch Hale telescope at the Palomar Observatory. The DBSP spectrum was reduced using a PyRAF-based pipeline (Bellm & Sesar 2016). We obtained a final spectrum one month later using LRIS.

The spectral sequence obtained via our follow-up for ZTF18aaqjovh is shown in Figure 3, compared to spectra of SN 1998bw at similar phases post-explosion. We used our spectra to estimate the photospheric velocity of ZTF18aaqjovh as a function of time. In typical Ic SNe, photospheric velocity is measured using the width of the Fe II $\lambda 5169$ line (e.g., Branch et al. 2002). However, due to the high velocities in Ic-BL SNe, the Fe II $\lambda 5169$ line is blended with the nearby Fe II $\lambda\lambda$ 4924,5018 lines. So, to perform our velocity measurements, we use the publicly available code²² based on the method in

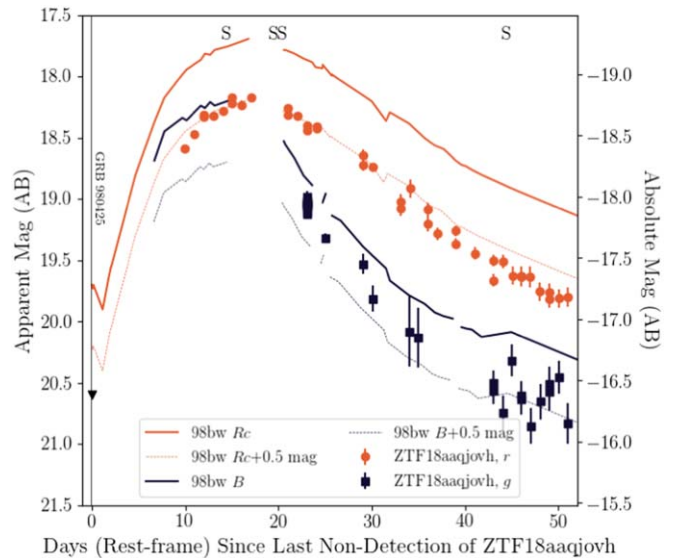


Figure 2. Optical light curve of ZTF18aaqjovh, corrected for Milky Way extinction, with P48 *r*-band in orange circles and P48 *g*-band in black squares. The light curve of SN 1998bw from Table 2 of Clocchiatti et al. (2011) is shown for comparison as thick black (*B*-band) and thick orange (*Rc*-band) lines, shifted to the redshift of ZTF18aaqjovh and also corrected for Milky Way extinction. The same SN 1998bw light curves are shifted by 0.4 mag for closer comparison and are shown as thin dotted lines. The vertical line on the left-hand side indicates the relative time of the GRB 980425, the low-luminosity gamma-ray burst associated with SN 1998bw. The epochs of optical spectra of ZTF18aaqjovh are marked with “S” along the top of the figure.

Table 2
Spectroscopic Observations of ZTF18aaqjovh

Date (MJD)	Δt (days)	Tel.+Instr.	Exp. Time (s)	v_{ph} (10^4 km s ⁻¹)
58247.359	14	P60+SEDM	1800	2.12 ± 0.46
58252.322	19	Keck I+LRIS	920	1.74 ± 0.28
58253.977	20	NOT+ALFOSC	2400	1.84 ± 0.54
58277.253	44	P200+DBSP	2700	1.12 ± 0.33
58338.249	105	Keck I+LRIS	1720	N/A

Modjaz et al. (2016), which convolves a Ic spectrum with Gaussian functions of varying widths until a best match is reached. For the SEDM measurements, we subtracted the contribution to the velocity from the resolution of the spectrograph, assuming that $\Delta v_{obs}^2 = \Delta v_{real}^2 + \Delta v_{inst}^2$ and that $\Delta v_{inst} = 3000$ km s⁻¹. The resulting velocities are listed in Table 2, and we show the velocity evolution compared to other Ic-BL SNe in Figure 4.

2.3. Radio Observations

Upon classifying ZTF18aaqjovh as a Type Ic-BL SN (Section 2.2) we triggered the NSF’s Karl G. Jansky VLA (Perley et al. 2011) for radio follow-up observations under the program VLA/18A-176 (PI: A. Corsi). A log of our observations is provided in Table 3.

We observed the field of ZTF18aaqjovh with the VLA over several epochs using the S, C, and Ku bands. We used J1150 +2417 as our complex gain calibrator, and 3C286 as our flux density and bandpass calibrator. Data were calibrated using the VLA calibration pipeline available in the Common Astronomy Software Applications (CASA; McMullin et al. 2007). After

²¹ <http://www.not.iac.es/instruments/alfosc/>

²² <https://github.com/nyusngroup/SESNspectraLib>

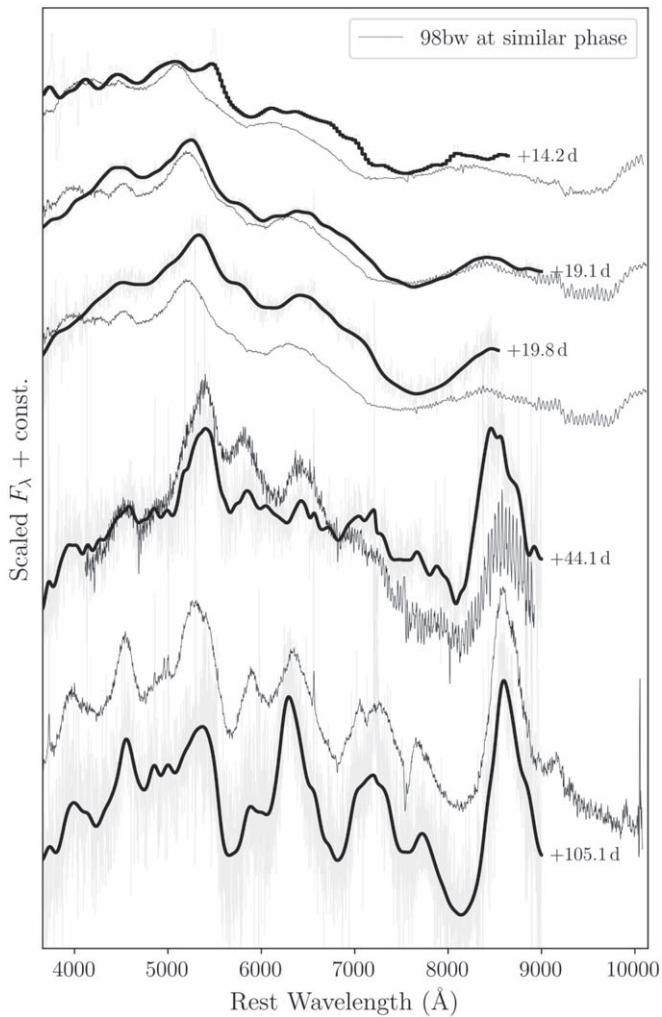


Figure 3. Optical spectra of ZTF18aaqjovh. Full spectra are shown in light gray and smoothed spectra are shown in thick black lines. For comparison, we show spectra of SN 1998bw at similar phases as thin black lines. The SN 1998bw spectra were taken from the Open Supernova Catalog (<https://sne.space/>) and are originally from Patat et al. (2001).

(The data used to create this figure are available.)

calibration, we inspected the data manually for further flagging. Images of the field were created using the CLEAN algorithm (Högbom 1974) available in CASA.

In our VLA images, we found a radio point source consistent with the optical position of ZTF18aaqjovh. Although the radio emission from this source remained fairly constant during the three epochs of our monitoring in C-band (see Table 3), its transient nature was confirmed by a nondetection about 280 days after the SN optical discovery. The radio peak flux densities are reported in Table 3. Flux density errors are calculated as the quadrature sum of the image rms and a fractional 5% absolute flux calibration error.

The radio light curve of ZTF18aaqjovh is shown in Figure 5, compared to several other Ic-BL SNe. At the distance of ZTF18aaqjovh, the 6 GHz radio luminosity density at $\Delta t \approx 20$ days since explosion is 2×10^{27} erg s⁻¹ Hz⁻¹. This is over an order of magnitude fainter than SN 1998bw at a similar epoch, and most similar to the luminosity of iPTF17cw at similar frequencies.

2.4. X-Ray Observations

A log of our X-ray observations is provided in Table 4.

On 2018 May 31 UT, we obtained a 2.5 ks target-of-opportunity observation of the position of ZTF18aaqjovh with the X-ray Telescope (XRT) on board the Neil Gehrels Swift Observatory (Burrows et al. 2005). We built the XRT light curve using the online generator (Evans et al. 2009). On the web form,²³ we used the default values except for Try to centroid?, which was set to No. The source was not detected with a 3σ upper limit of 7.2×10^{-3} cps. To convert the upper limit from count rate to flux, we assumed a Galactic neutral hydrogen column density²⁴ of $n_H = 1.37 \times 10^{20}$ cm⁻² and a power-law spectrum $f \propto E^{-\Gamma}$ where f is flux (photons cm⁻² s⁻¹), E is energy, and $\Gamma = 2$ is the photon index. This gives an unabsorbed upper-limit on the 0.3–10 keV flux of 2.3×10^{-13} erg cm⁻² s⁻¹, corresponding to a luminosity of 1.7×10^{42} erg s⁻¹.

We also obtained two epochs of observations of ZTF18aaqjovh with the Advanced CCD Imaging Spectrometer (ACIS; Garmire et al. 2003) on the Chandra X-ray Observatory via our approved program (No. 19500451, PI: Corsi). The first epoch began at 11:07 on 2018 May 28 UT ($\Delta t \approx 33$ days) under ObsId 20315 (integration time 9.93 ks), and the second began at 11:10 on 2018 July 24 UT ($\Delta t \approx 90$ days) under ObsId 20316. No X-ray emission was detected at the location of ZTF18aaqjovh in either epoch, with a 90% upper limit on the 0.5–7.0 keV count rate of 2.52×10^{-4} ct s⁻¹ and 2.32×10^{-4} ct s⁻¹, respectively. For the same Galactic n_H and power-law source model that we used in the Swift data, we obtain an upper limit on the unabsorbed 0.3–10 keV flux of 3.4×10^{-15} erg s⁻¹ cm⁻² in the first epoch and 3.1×10^{-15} erg s⁻¹ cm⁻² in the second epoch. At the distance of ZTF18aaqjovh, these correspond to upper limits on the X-ray luminosity of 2.5×10^{40} and 2.3×10^{40} erg s⁻¹. These upper limits are compared with the X-ray luminosity of radio-loud Ic-BL SNe in Figure 6.

2.5. Search for Gamma-Rays

We searched for any gamma-ray burst (GRB) coincident with the position and estimated time of first light of ZTF18aaqjovh. As shown in Figure 2 and discussed in more detail in Section 3.1, we can use the relative time between GRB 980425 and the r -band peak of SN 1998bw to estimate the time of a GRB associated with ZTF18aaqjovh. If this relative time is the same between the two SNe, then the associated GRB would have been approximately at the time of the last nondetection ($t_0 \approx 2018$ April 25 UT), 10 days prior to the first detection on 2018 May 5 UT.

To be conservative, we set our search window to be $t_0 \pm 10$ days. In Table 5 we list all 20 GRBs detected in this window. Of the 20, all but one are ruled out based on the position of the SN. The only possible counterpart is a GRB on 2018 May 3 03:41:01 ($\Delta t = 8$) detected by Konus-Wind while Fermi/GBM was offline. The duration of this burst was 35 s. Modeling the spectrum with a cutoff power-law model with $E_p = 107^{+64}_{-25}$ keV and 20–1500 keV fluence 2×10^{-6} erg cm⁻² we obtain an $L_{\text{iso}} = 8 \times 10^{47}$ erg s⁻¹, which is typical of LLGRBs (Cano et al. 2017).

²³ https://www.swift.ac.uk/user_objects/

²⁴ <https://heasarc.gsfc.nasa.gov/cgi-bin/Tools/w3nh/w3nh.pl>

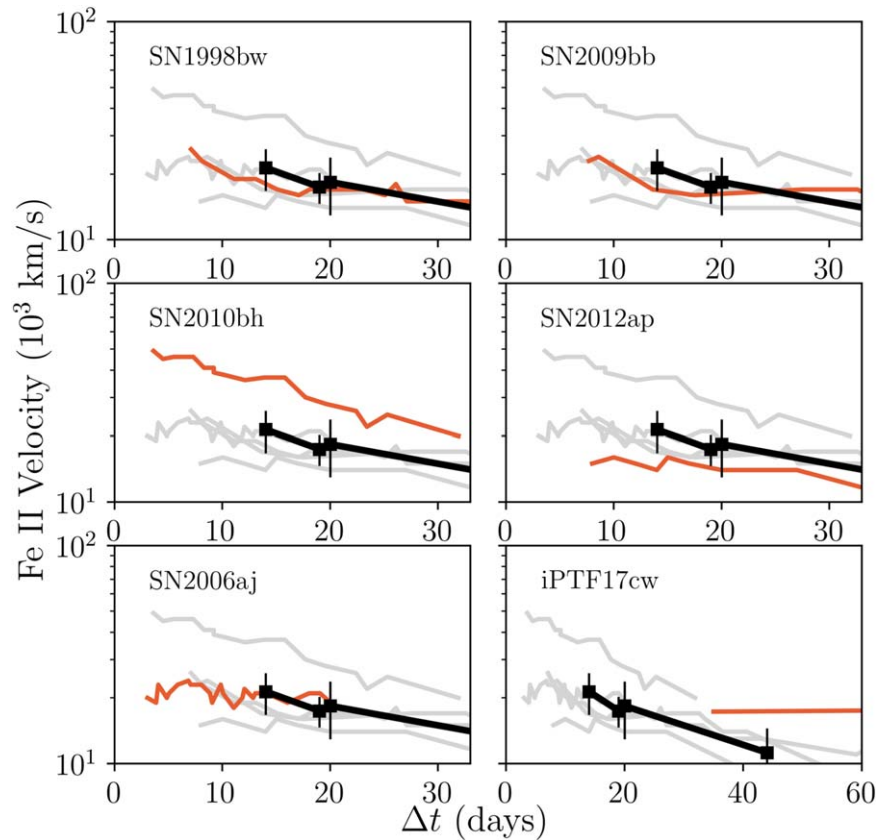


Figure 4. Evolution of the photospheric velocity of ZTF18aaqjovh over time as measured from Fe II absorption features in the Ic-BL spectra. For comparison, we show the velocity evolution of several LLGRB-SNe (SN 1998bw/GRB 908425, SN 2010bh/GRB 100316D, and SN 2006aj/GRB 060218) and radio-loud relativistic SNe lacking a coincident GRB detection (SN 2009bb, SN 2012ap, and iPTF 17cw). Each panel shows measurements for ZTF18aaqjovh as black squares, the population of comparison events as light gray lines in the background, and one comparison SN highlighted in orange. Data were taken from Modjaz et al. (2016) and explosion times were estimated from Galama et al. (1998), Campana et al. (2006), Soderberg et al. (2010), Bufano et al. (2012), Milisavljevic et al. (2015), and Corsi et al. (2014).

Table 3
Radio Flux Density Measurements of ZTF18aaqjovh

Start Date (UT)	Time on-source (hr)	Δt (days)	$S_{3 \text{ GHz}}$ ($\mu \text{ Jy}$)	$S_{6 \text{ GHz}}$ ($\mu \text{ Jy}$)	$S_{15 \text{ GHz}}$ ($\mu \text{ Jy}$)	Array Config.
2018 May 11	0.67	16	...	32.5 ± 7.1	...	A
2018 May 16	0.67	21	26.0 ± 6.9	...	15.1 ± 5.2	A
2018 May 17	0.67	22	...	29.6 ± 5.3	...	A
2018 May 29	0.67	34	...	26.6 ± 5.4	...	A
2018 May 31	1.5	36	34.6 ± 4.8	A
2019 Jan 26	1.5	276	...	$\lesssim 15$...	C

However, due to the coarse localization and the implication that the light curve of ZTF18aaqjovh increased to peak brightness much more steeply than the light curve of SN 1998bw, we consider the association with the GRB on May 3 to be unlikely. Assuming it is not related, we can set a limit on the fluence and corresponding isotropic equivalent energy of a prompt burst associated with ZTF18aaqjovh. The Interplanetary Network (IPN) has essentially a 100% duty cycle across the sky, and detects GRBs with $E_{\text{pk}} > 20 \text{ keV}$ down to $6 \times 10^{-7} \text{ erg cm}^{-2}$ at 50% efficiency (Hurley et al. 2010, 2016). Using Konus-Wind waiting mode data near t_0 and assuming a typical GRB spectrum (a Band function with $\alpha = -1$, $\beta = -2.5$, and $E_p = 300 \text{ keV}$; Band et al. 1993; Preece et al. 2000), we estimate a peak limiting flux of $2.1 \times 10^{-7} \text{ erg cm}^{-2} \text{ s}^{-1}$ (20–1500 keV, 2.944 s scale). At the

distance of ZTF18aaqjovh, this corresponds to an upper limit on a GRB peak luminosity of $L_{\text{iso}} \approx 1.6 \times 10^{48} \text{ erg s}^{-1}$, two orders of magnitude less luminous than classical GRBs but similar to LLGRBs (Cano et al. 2017). We note that the IPN would not be sensitive to LLGRBs such as LLGRB 060218 associated with SN 2006aj (Cano et al. 2017) because of their soft spectra ($E_{\text{pk}} < 20 \text{ keV}$ for 060218).

3. Analysis and Discussion

3.1. Modeling the Optical Light Curve

As shown in Figure 2, the r -band light curve of ZTF18aaqjovh declines slightly faster than the light curve of SN 1998bw, and is 0.4 mag fainter. For an SN with an optical light curve powered by radioactive decay, the “stretch” (width)

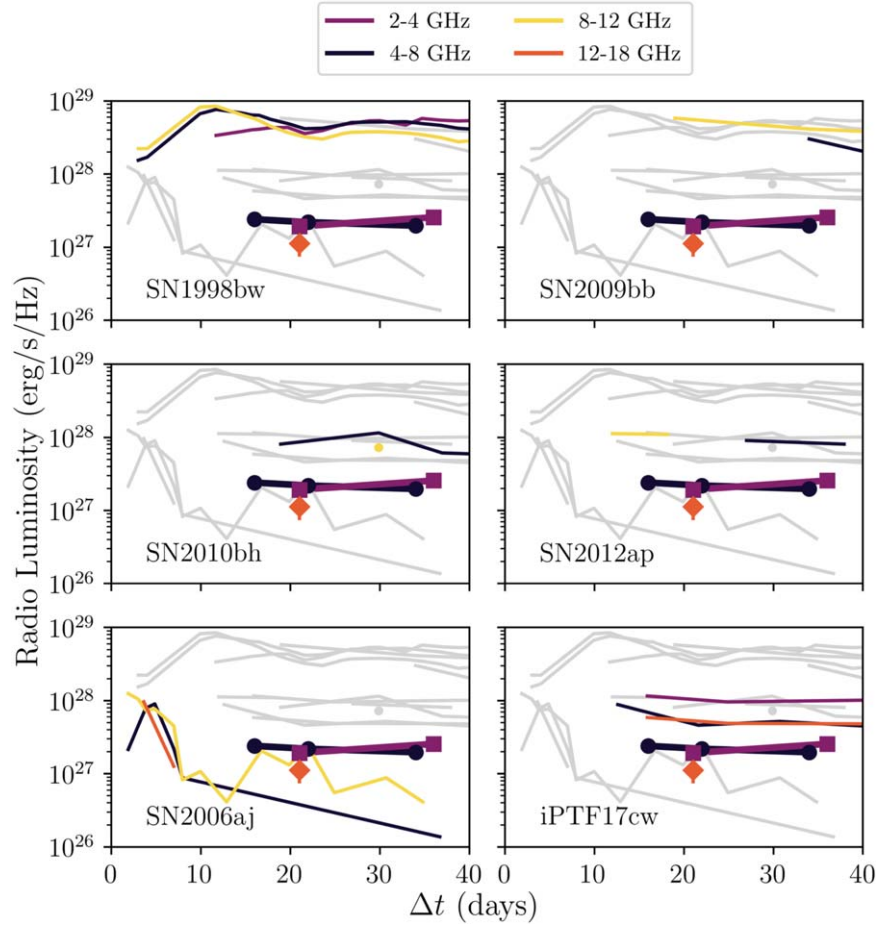


Figure 5. Radio light curve of ZTF18aaqjovh compared with LLGRB-SNe (SN 1998bw/GRB 980425, SN 2010bh/GRB 100316D, and SN 2006aj/GRB 060218) and relativistic SNe (SN 2009bb, SN 2012ap, and iPTF17cw). Each panel shows observations of ZTF18aaqjovh (connected symbols), the population of comparison events as light gray lines in the background, and one SN highlighted as colored lines for comparison. Note that ZTF18aaqjovh lacks data in the 8–12 GHz range. Data were taken from Kulkarni et al. (1998), Soderberg et al. (2010), Chakraborti et al. (2015), Margutti et al. (2014), Soderberg et al. (2006), and Corsi et al. (2017).

Table 4
X-Ray Observations of ZTF18aaqjovh

Start Date (UT)	Δt (days)	Instr.	Int. (ks)	Flux ($\text{erg s}^{-1} \text{cm}^{-2}$)
2018 May 28 11:07:06	33	Chandra/ACIS	9.93	$< 3.4 \times 10^{-15}$
2018 May 31 00:33:57	36	Swift/XRT	2.5	$< 2.3 \times 10^{-13}$
2018 Jul 24 11:10:42	90	Chandra/ACIS	9.93	$< 3.1 \times 10^{-15}$

of the light curve scales with the kinetic energy and ejecta mass as (Valenti et al. 2008; Lyman et al. 2016)

$$\tau_m \propto \left(\frac{M_{\text{ej}}^3}{E_k} \right)^{1/4}, \quad (1)$$

where τ_m is the width of the light curve, M_{ej} is the ejecta mass, and E_k is the kinetic energy of the explosion. The degeneracy between M_{ej} and E_k is broken by the photospheric velocity (see Equation (2) in Lyman et al. 2016):

$$v_{\text{ph}}^2 = \frac{5}{3} \frac{2E_k}{M_{\text{ej}}}. \quad (2)$$

As shown in Figure 2 and Figure 4, ZTF18aaqjovh has a photospheric velocity close to that of SN 1998bw, and its light curve is narrower. So, we expect the ejecta mass and

kinetic energy of ZTF18aaqjovh to be slightly smaller to that of SN 1998bw, which had $M_{\text{ej}} \approx 4.4^{+1.2}_{-0.8} M_{\odot}$ and $E_k \approx 9.9^{+3.8}_{-2.2} \times 10^{51}$ erg, respectively (Lyman et al. 2016), values typical of Ic-BL SNe from untargeted surveys (Taddia et al. 2019).

Finally, assuming that the dominant powering mechanism for the optical light curve is radioactive decay, we have the following energy deposition rate from ^{56}Ni (Kasen 2017):

$$L^{56\text{Ni}}(t) = 2 \times 10^{43} \left(\frac{M_{\text{Ni}}}{M_{\odot}} \right) [3.9e^{-t/\tau_{\text{Ni}}} + 0.678(e^{-t/\tau_{\text{Co}}} - e^{-t/\tau_{\text{Ni}}})] \text{erg s}^{-1}, \quad (3)$$

where the decay lifetimes of ^{56}Ni and ^{56}Co are $\tau_{\text{Ni}} = 8.8$ days and $\tau_{\text{Co}} = 113.6$ days, respectively. Arnett’s law (Arnett 1982) states that the instantaneous energy deposition rate is equal to the SN luminosity at peak. Under this assumption, the peak luminosity is simply equal to $L^{56\text{Ni}}$ at that time, so is directly proportional to M_{Ni} .

Taking $L \approx \nu L_{\nu} \approx 6.9 \times 10^{42}$ erg s $^{-1}$ at peak light ($t \approx 15$ days) we find that $M_{\text{Ni}} \approx 0.3 M_{\odot}$. For reference, the nickel mass of SN 1998bw has been estimated to be $M_{\text{Ni}} \approx 0.54^{+0.08}_{-0.07} M_{\odot}$ (Lyman et al. 2016). These values are typical for GRB-SNe (Cano et al. 2017) and for Ic-BL SNe in general (Taddia et al. 2019).

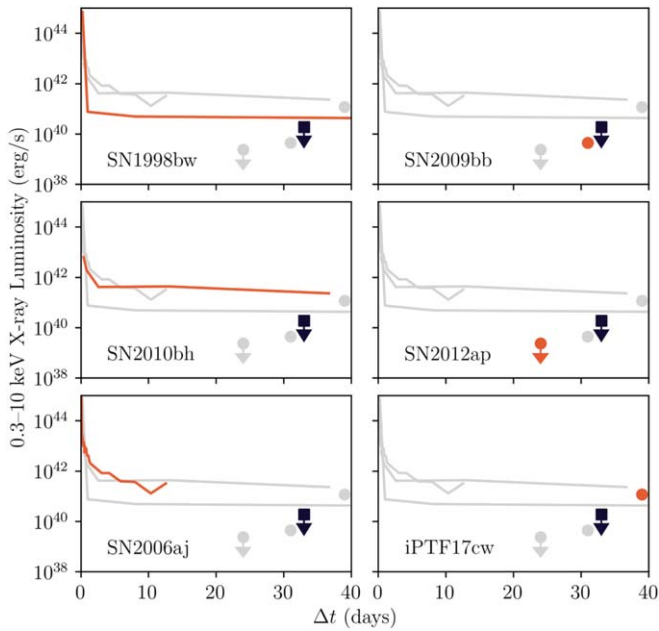


Figure 6. Upper limit on the X-ray luminosity of ZTF18aaqjovh from our first Chandra observation (black square) compared to the X-ray luminosity at similar epochs of LLGRBs (SN 1998bw, SN 2010bh, and SN 2006aj) and Ic-BL SNe with relativistic outflows discovered independently of a γ -ray trigger (iPTF17cw, SN 2009bb, and SN 2012ap). Each panel shows the full set of comparison events in light gray, with one event highlighted in orange. Data were taken from Corsi et al. (2017), Campana et al. (2006), and Margutti et al. (2014).

3.2. Properties of the Fastest (Radio-emitting) Ejecta

As shown in Figure 5, the radio luminosity of ZTF18aaqjovh is between that of SN 2006aj and that of iPTF17cw. Due to the faintness of the SN it is unfortunately difficult to measure the true rate of change of the flux, but the slow temporal evolution of the 3–6 GHz flux during the first four epochs of observation ($\Delta t = 16$ days to $\Delta t = 36$ days) may imply that the synchrotron self-absorption (SSA) frequency is passing through these frequencies at this time. This is supported by the 3–15 GHz observations at $\Delta t = 21$ –22 days, which suggest that the SSA peak is below 15 GHz and close to 3–6 GHz. Altogether, we conclude that the SSA peak is 3–15 GHz at $\Delta t \approx 20$ days, and that the peak flux is 20–30 μ Jy.

With these estimates of the SSA peak frequency and peak flux, we use the framework laid out in Chevalier (1998) to estimate the shock energy U (the amount that has been converted into pressure by the ambient medium), the ambient density, and the mean shock velocity at $\Delta t \sim 20$ days. The assumption is that the synchrotron spectrum arises from a population of relativistic electrons with a power-law number distribution in Lorentz factor γ_e and some minimum Lorentz factor γ_m :

$$\frac{dN(\gamma_e)}{d\gamma_e} \propto \gamma_e^{-p}, \gamma_e \geq \gamma_m. \quad (4)$$

For typical radio SNe, $2.5 < p < 3$ (Jones & Ellison 1991). Here we assume $p \approx 3$, as in Chevalier (1998). Under this assumption, expressions for the shock radius and magnetic field strength are given in Equations (13) and (14) of Chevalier (1998). The magnetic field strength can then be used to estimate the magnetic energy density, assuming that equal

Table 5
Gamma-Ray Bursts within 10 Days of the Estimated Time of First Light of ZTF18aaqjovh

Date (UT)	Name	Δt (days)	Instr.	Pos.	Verdict
2018 Apr 16	180416D	−9	KAI	N	N(a)
2018 Apr 16	180416A	−9	KGI	113.65, +49.120	N(b)
2018 Apr 16	180416B	−9	KGAC	354.233, +78.433	N(b)
2018 Apr 17		−8	K	S	N(c)
2018 Apr 20		−5	KG	93.510, −28.320	N(b)
2018 Apr 20		−5	KGI	83.230, −25.250	N(b)
2018 Apr 21		−4	K	N	N(c)
2018 Apr 23		−2	KGI	208.680, +9.840	N(b)
2018 Apr 25	180425A	0	KS	64.452, −32.952	N(b)
2018 Apr 26		1	KGI	251.240, +81.390	N(b)
2018 Apr 26		1	KG	202.410, +58.170	N(b)
2018 Apr 26		1	K	N	N(c)
2018 Apr 26		1	K	S	N(b)
2018 Apr 27	180427A	2	KGI	283.330, +70.300	N(b)
2018 Apr 28		3	KGI	92.120, +54.780	N(b)
2018 Apr 28		3	K	N	N(c)
2018 Apr 29		4	KI	S	N(b)
2018 May 3		8	K	N	Y
2018 May 4		9	KGI	220.230, +38.720	N(b)
2018 May 4	180504A	9	KSI	331.144, −14.658	N(b)

Note. In the Position column, N and S mean that the position is localized to the northern and southern ecliptic hemispheres, respectively. In the Instrument column, K means Konus-Wind, A means Astrosat, I means INTEGRAL SPI-ACS, G means Fermi/GBM, and S means Swift/BAT. In the Verdict column, N means that an association is ruled out because (a) the SN position was Earth-occulted for Astrosat and GBM, (b) the SN position is inconsistent with the localized burst position, or (c) the SN position was visible to GBM but not detected. Y means that an association is possible.

amounts of energy are partitioned into electrons, magnetic fields, and protons (Soderberg et al. 2010).

These relations between observables and physical properties are summarized in Figure 7, adapted from Ho et al. (2019). The mean velocity of the shock we derive for ZTF18aaqjovh is $v = 0.06$ – $0.4c$. So, the outflow associated with ZTF18aaqjovh could have been as fast as that observed in the GRB-associated SN 2010bh. The implied mass-loss rate is 0.1 – $3 \times 10^{-4}(v_w/1000 \text{ km s}^{-1}) M_\odot \text{ yr}^{-1}$, which could be as high as that of the strongly CSM-interacting SN PTF 11qej (Corsi et al. 2014).

3.3. Modeling the Radio to X-Ray SED

In SN explosions, the shockwave that accelerates electrons into a power-law distribution and produces synchrotron radiation, detected as radio emission, can also produce X-rays (Chevalier & Fransson 2006) via several mechanisms. X-rays can have the same origin as the radio emission (lying along the same synchrotron spectrum). However, X-rays can also arise from inverse Compton scattering of the optical photons by the electrons producing the radio emission (Chevalier & Fransson 2006, 2017). For a number of Ic-BL SNe, it seems that the simple synchrotron scenario is insufficient to explain the radio and X-ray observations—in other words, there is an excess of

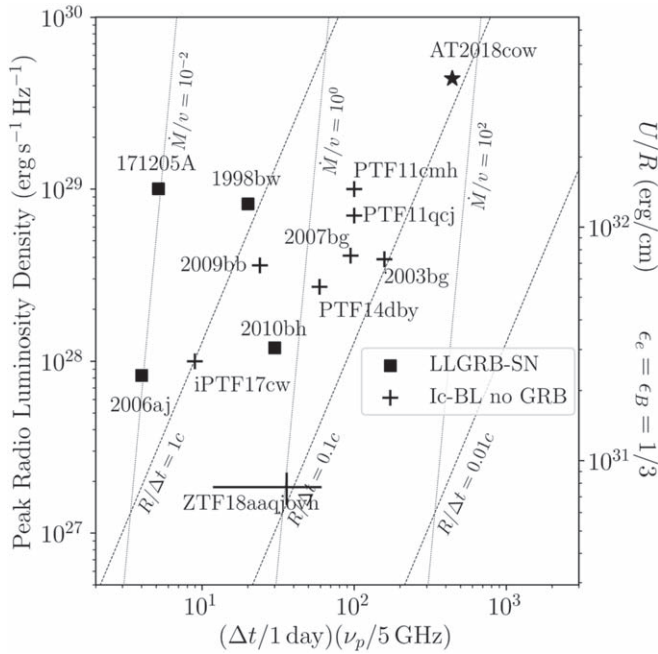


Figure 7. Peak radio luminosity of ZTF18aaqjovh compared to other energetic stellar explosions; see Chevalier (1998), Soderberg et al. (2010), and Ho et al. (2019). In Ho et al. (2019) we showed that the peak luminosity is directly proportional to U/R , the energy swept up per unit radius; we display this value on the right-hand side. Error bars reflect the estimated SSA peak (20–30 μ Jy, 3–15 GHz) at $\Delta t \approx 20$ days. Lines of constant velocity are shown, as well as lines of constant mass-loss rate (scaled to wind velocity) in units of $10^{-4} M_{\odot} \text{yr}^{-1}/1000 \text{ km s}^{-1}$. The radio luminosity for GRB 171205A was taken from VLA observations reported by Laskar et al. (2017) but we note that this is a lower limit in luminosity and in peak frequency because the source was heavily self-absorbed at this epoch. The radio luminosity for other sources is from, or derived using data from, Soderberg et al. (2010), Kulkarni et al. (1998), Soderberg et al. (2006), Margutti et al. (2013), Corsi et al. (2014, 2017), Salas et al. (2013), and Soderberg et al. (2005, 2006).

X-ray emission (Soderberg et al. 2006; Margutti et al. 2013; Corsi et al. 2014).

As described in Section 2.4, we do not detect X-ray emission from ZTF18aaqjovh, corresponding to upper limits of $L_X < 3.4 \times 10^{40} \text{ erg s}^{-1}$ at $\Delta t \sim 33$ days and $L_X < 3.1 \times 10^{40} \text{ erg s}^{-1}$ at $\Delta t \sim 90$ days. At $\Delta t \sim 33$ days, this is smaller than the luminosity of X-ray emission associated with iPTF17cw, SN 1998bw (GRB 980425), and SN 2010bh (GRB 031203) at a similar epoch. The 0.3–10 keV luminosity of SN 2010bh at $\Delta t = 38$ days was $2.4 \times 10^{41} \text{ erg s}^{-1}$ (Margutti et al. 2014), which was already the least X-ray luminous LLGRB at this phase (second only to GRB 980425). Due to a lack of data later than 10 days we cannot rule out a luminosity similar to SN 2006aj, SN 2009bb, and SN 2012ap (Margutti et al. 2014).

Figure 8 shows the radio luminosity and X-ray upper limit at $\Delta t \approx 33$ days, from our observations of ZTF18aaqjovh with the VLA and Chandra on 2018 May 28–29 UT. The spectral index is constrained to be $\beta < -0.6$ where $L_{\nu} \propto \nu^{\beta}$. A common optically thin spectral index for radio SNe is $\beta \sim -0.5$ to -1 (Chevalier 1998) where $F_{\nu} \propto \nu^{\beta}$. Above the cooling frequency, this steepens to $\beta \sim -1$ or $\beta \sim -1.5$. Thus we cannot conclude whether there is X-ray emission from an extension of the synchrotron spectrum, or whether there is an excess from some other mechanism such as cosmic-ray-dominated shocks (Chevalier & Fransson 2006), which has been observed in a number of engine-driven SNe including

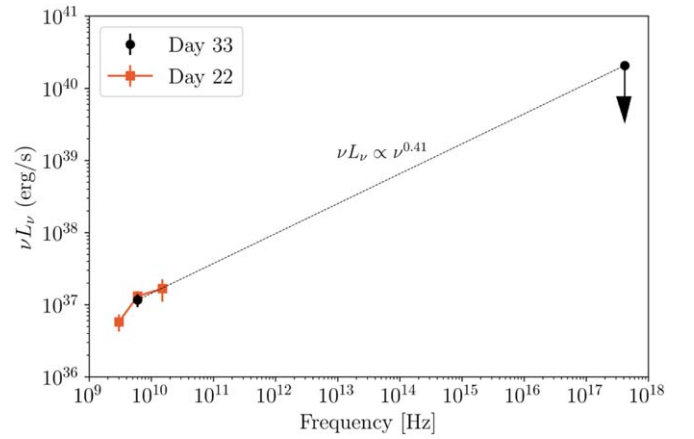


Figure 8. Radio luminosity and upper limit on X-ray luminosity of ZTF18aaqjovh at $\Delta t \approx 33$ days. From these measurements, we constrain the spectral index from the radio to X-ray frequencies to be $\beta < -0.6$ where $L_{\nu} \propto \nu^{\beta}$.

iPTF17cw ($\beta = -0.6$; Corsi et al. 2017), GRB 060218 ($\beta = -0.5$; Soderberg et al. 2006), and GRB 100316D ($\beta < -0.6$; Margutti et al. 2014).

3.4. Gamma-Ray Burst

In Section 2.5 we searched for coincident GRBs and found one possible counterpart, although the association is highly unlikely due to the close proximity of the burst time with the first detection of the light curve.

Here we work under the hypothesis that ZTF18aaqjovh was associated with a GRB that we missed, and attempt to derive possible constraints on the γ -ray emission based on the SN properties. From four GRB-SNe, Li (2006) found the following relation between the peak spectral energy of the GRB and the peak bolometric luminosity of the associated SN:

$$E_{\gamma, \text{peak}} = 90.2 \text{ keV} \left(\frac{L_{\text{SN, peak}}}{10^{43} \text{ erg s}^{-1}} \right)^{4.97}. \quad (5)$$

From the peak of the r -band light curve of ZTF18aaqjovh, we can estimate $L_{\text{SN, peak}} \approx \nu f_{\nu} \approx 1.7 \times 10^9 L_{\odot}$, which gives $E_{\gamma, \text{peak}} \approx 15 \text{ keV}$. Using the so-called Amati relationship between a GRB peak energy and its isotropic equivalent energy (Amati 2006; Li 2006):

$$E_{\gamma, \text{peak}} = 97 \text{ keV} \left(\frac{E_{\gamma, \text{iso}}}{10^{52} \text{ erg s}^{-1}} \right)^{0.49}, \quad (6)$$

we find an expected $E_{\text{iso}} \approx 2 \times 10^{50} \text{ erg}$ for a potential GRB associated with ZTF18aaqjovh. These values of $E_{\gamma, \text{peak}}$ and E_{iso} are similar to what has been measured for LLGRBs (Cano et al. 2017), and would not have been detectable by the IPN.

4. Summary and Conclusions

We have presented optical, X-ray, and radio observations of the Ic-BL SN ZTF18aaqjovh, discovered by ZTF as part of our campaign with the VLA to search for engine-driven explosions. ZTF18aaqjovh shares a number of features in common with relativistic SNe: an optical light curve similar to SN 1998bw and early peaking radio emission similar to iPTF17cw. The limits on X-ray and gamma-ray emission rule out a classical

GRB but cannot rule out an LLGRB. Due to the low signal-to-noise of our measurements, we can only constrain the velocity of the forward shock to be 0.06–0.4 c . Thus, this is at most a mildly relativistic explosion, and we have no definitive evidence of a long-lived central engine.

From radio follow-up observations of Ic-BL SNe discovered by PTF and now ZTF, it has become clear that emission as luminous as that accompanying SN 1998bw is rare. Without a GRB trigger it is challenging to discover explosions similar to SN 2006aj, which had a low-frequency radio light curve that peaked within the first five days and faded more quickly than the light curve of SN 1998bw. In the case of ZTF18aaqjovh, X-ray observations within the first 10 days may have enabled us to detect an X-ray light curve like that accompanying SN 2006aj, but we were unable to observe with Swift due to the proximity of ZTF18aaqjovh to the Sun at the time.

At present, Ic-BL SNe are discovered and classified via brute-force spectroscopy, so unless they are very nearby they are typically not recognized until a week after explosion. It would be useful to develop strategies for discovering Ic-BL SNe earlier in their evolution, perhaps based on the properties of their host environment, or—in higher-cadence surveys—from the presence of an early (<1 day) peak in the optical light curve, like that seen in SN 2006aj and SN 1998bw. These could perhaps be distinguished from double-peaked light curves of other SN progenitors (e.g., Fremling et al. 2019b) by the luminosity of this first peak, if the redshift to the SN is known.

The data are publicly available via WISEREP, an interactive repository of supernova data (Yaron & Gal-Yam 2012). The code to produce the figures in this paper has been released under doi:10.5281/zenodo.3634931.

We would like to thank the anonymous referee for taking the time to do a thorough reading of the manuscript, and for providing detailed and useful comments. A.Y.Q.H. thanks Kevin Hurley for maintaining the IPN master burst list (<http://www.ssl.berkeley.edu/ipn3/masterli.html>) that was used to compile Table 6, and Daniel Goldstein and Yuhan Yao (Caltech) for useful discussions regarding ZTF photometry.

Based on observations obtained with the Samuel Oschin Telescope 48 inch and the 60 inch Telescope at the Palomar Observatory as part of the Zwicky Transient Facility project. ZTF is supported by the National Science Foundation under grant No. AST-1440341 and a collaboration including Caltech, IPAC, the Weizmann Institute for Science, the Oskar Klein Center at Stockholm University, the University of Maryland, the University of Washington, Deutsches Elektronen-Synchrotron and Humboldt University, Los Alamos National Laboratories, the TANGO Consortium of Taiwan, the University of Wisconsin at Milwaukee, and Lawrence Berkeley National Laboratories. Operations are conducted by COO, IPAC, and UW. This work made use of data supplied by the UK Swift Science Data Centre at the University of Leicester. This work made use of the data products generated by the NYU SN group, and released under Bianco et al. (2016), available at <https://github.com/nyusgroup/SESNspectraLib>. SED Machine is based upon work supported by the National Science Foundation under grant No. 1106171. The ZTF forced-photometry service was funded under the Heising-Simons Foundation grant #12540303 (PI: Graham). Partially based on observations made with the Nordic Optical Telescope, operated by the Nordic Optical Telescope Scientific Association at the

Observatorio del Roque de los Muchachos, La Palma, Spain, of the Instituto de Astrofísica de Canarias. The data presented here were obtained in part with ALFOSC, which is provided by the Instituto de Astrofísica de Andalucía (IAA) under a joint agreement with the University of Copenhagen and NOTSA. The National Radio Astronomy Observatory is a facility of the National Science Foundation operated under cooperative agreement by Associated Universities, Inc.

A.Y.Q.H. is supported by a National Science Foundation Graduate Research Fellowship under grant No. DGE1144469. A.C. acknowledges support from the National Science Foundation CAREER award #1455090. A.C. and A.Y.Q.H. acknowledge support from the Chandra GI award #19500451. This work was partially supported by the GROWTH project funded by the National Science Foundation under PIRE grant No. 1545949. A.A.M. is funded by the Large Synoptic Survey Telescope Corporation, the Brinson Foundation, and the Moore Foundation in support of the LSSTC Data Science Fellowship Program; he also receives support as a CIERA Fellow by the CIERA Postdoctoral Fellowship Program (Center for Interdisciplinary Exploration and Research in Astrophysics, Northwestern University). C.F. gratefully acknowledges support of his research by the Heising-Simons Foundation (#2018-0907).

ORCID iDs

Anna Y. Q. Ho  <https://orcid.org/0000-0002-9017-3567>
 Alessandra Corsi  <https://orcid.org/0000-0001-8104-3536>
 S. Bradley Cenko  <https://orcid.org/0000-0003-1673-970X>
 S. R. Kulkarni  <https://orcid.org/0000-0001-5390-8563>
 Dmitry D. Frederiks  <https://orcid.org/0000-0002-1153-6340>
 Christoffer Fremling  <https://orcid.org/0000-0002-4223-103X>
 V. Zach Golkhou  <https://orcid.org/0000-0001-8205-2506>
 Matthew J. Graham  <https://orcid.org/0000-0002-3168-0139>
 Tiara Hung  <https://orcid.org/0000-0002-9878-7889>
 Thomas Kupfer  <https://orcid.org/0000-0002-6540-1484>
 Russ R. Laher  <https://orcid.org/0000-0003-2451-54824>
 Frank J. Masci  <https://orcid.org/0000-0002-8532-9395>
 Adam A. Miller  <https://orcid.org/0000-0001-9515-478X>
 James D. Neill  <https://orcid.org/0000-0002-0466-1119>
 Reed Riddle  <https://orcid.org/0000-0002-0387-370X>
 Ben Rusholme  <https://orcid.org/0000-0001-7648-4142>
 Jesper Sollerman  <https://orcid.org/0000-0003-1546-6615>
 Maayane T. Soumagnac  <https://orcid.org/0000-0001-6753-1488>
 Dmitry S. Svinkin  <https://orcid.org/0000-0002-2208-2196>
 David L. Shupe  <https://orcid.org/0000-0003-4401-0430>

References

- Ahn, C. P., Alexandroff, R., Allende Prieto, C., et al. 2014, *ApJS*, 211, 17
 Alam, S., Albareti, F. D., Allende Prieto, C., et al. 2015, *ApJS*, 219, 12
 Amati, L. 2006, *MNRAS*, 372, 233
 Amati, L., Frontera, F., Tavani, M., et al. 2002, *A&A*, 390, 81
 Arnett, W. D. 1982, *ApJ*, 253, 785
 Band, D., Matteson, J., Ford, L., et al. 1993, *ApJ*, 413, 281
 Barnes, J., Duffell, P. C., Liu, Y., et al. 2018, *ApJ*, 860, 38
 Bellm, E. C., Kulkarni, S. R., Barlow, T., et al. 2019a, *PASP*, 131, 068003
 Bellm, E. C., Kulkarni, S. R., Graham, M. J., et al. 2019b, *PASP*, 131, 018002
 Bellm, E. C., & Sesar, B. 2016, pyraf-dbsp: Reduction pipeline for the Palomar Double Beam Spectrograph, Astrophysics Source Code Library, ascl:1602.002
 Bersier, D., Fruchter, A. S., Strolger, L.-G., et al. 2006, *ApJ*, 643, 284

- Bianco, F. B., Liu, Y., & Modjaz, M. 2016, SESNSpectralLib: First Public Release, Version 1.0, Zenodo, doi:[10.5281/zenodo.58767](https://doi.org/10.5281/zenodo.58767)
- Blagorodnova, N., Neill, J. D., Walters, R., et al. 2018, *PASP*, **130**, 035003
- Blondin, S., & Tonry, J. L. 2007, *ApJ*, **666**, 1024
- Branch, D., Benetti, S., Kasen, D., et al. 2002, *ApJ*, **566**, 1005
- Bromberg, O., Nakar, E., & Piran, T. 2011, *ApJL*, **739**, L55
- Bufano, F., Pian, E., Sollerman, J., et al. 2012, *ApJ*, **753**, 67
- Burrows, D. N., Hill, J. E., Nousek, J. A., et al. 2005, *SSRv*, **120**, 165
- Campana, S., Mangano, V., Blustin, A. J., et al. 2006, *Natur*, **442**, 1008
- Cano, Z. 2013, *MNRAS*, **434**, 1098
- Cano, Z., Wang, S.-Q., Dai, Z.-G., & Wu, X.-F. 2017, *AdAst*, **2017**, 8929054
- Cappellaro, E., Mazzali, P. A., Benetti, S., et al. 1997, *A&A*, **328**, 203
- enko, S. B., Fox, D. B., Moon, D.-S., et al. 2006, *PASP*, **118**, 1396
- Chakraborti, S., Soderberg, A., Chomiuk, L., et al. 2015, *ApJ*, **805**, 187
- Chand, V., Banerjee, A., Gupta, R., et al. 2020, arXiv:2001.00648
- Chevalier, R. A. 1998, *ApJ*, **499**, 810
- Chevalier, R. A., & Fransson, C. 2006, *ApJ*, **651**, 381
- Chevalier, R. A., & Fransson, C. 2017, in *Handbook of Supernovae*, ed. R. A. Alsabti & P. Murdin (Cham: Springer), 875
- Clocchiatti, A., Suntzeff, N. B., Covarrubias, R., & Candia, P. 2011, *AJ*, **141**, 163
- Cook, D. O., Kasliwal, M. M., Van Sistine, A., et al. 2019, *ApJ*, **880**, 7
- Corsi, A., Cenko, S. B., Kasliwal, M. M., et al. 2017, *ApJ*, **847**, 54
- Corsi, A., Gal-Yam, A., Kulkarni, S. R., et al. 2016, *ApJ*, **830**, 42
- Corsi, A., Ofek, E. O., Gal-Yam, A., et al. 2014, *ApJ*, **782**, 42
- Dekany, R., Smith, R. M., Belicki, J., et al. 2016, *Proc. SPIE*, **9908**, 99085M
- D'Elia, V., Campana, S., D'Ai, A., et al. 2018, *A&A*, **619**, A66
- Djupvik, A. A., & Andersen, J. 2010, *ASSP*, **14**, 211
- Duev, D. A., Mahabal, A., Masci, F. J., et al. 2019, *MNRAS*, **489**, 3582
- Evans, P. A., Beardmore, A. P., Page, K. L., et al. 2009, *MNRAS*, **397**, 1177
- Fremming, C., Dugas, A., & Sharma, Y. 2019a, *Transient Name Server Classification Report 2019-892*
- Fremming, C., Ko, H., Dugas, A., et al. 2019b, *ApJL*, **878**, L5
- Fremming, C., Sollerman, J., Taddia, F., et al. 2016, *A&A*, **593**, A68
- Fremming, C., & Taggart, K. 2018, *Transient Name Server Discovery Report 2018-691*
- Fremming, U. C., Miller, A. A., Sharma, Y., et al. 2019c, arXiv:1910.12973
- Galama, T. J., Vreeswijk, P. M., van Paradijs, J., et al. 1998, *Natur*, **395**, 670
- Garmire, G. P., Bautz, M. W., Ford, P. G., Nousek, J. A., & Ricker, G. R., Jr. 2003, *Proc. SPIE*, **4851**, 28
- Graham, M. J., Kulkarni, S. R., Bellm, E. C., et al. 2019, *PASP*, **131**, 078001
- Hjorth, J., & Bloom, J. S. 2012, in *Gamma-Ray Bursts*, ed. C. Kouveliotou, R. A. M. J. Wijers, & S. Woosley (Cambridge: Cambridge Univ. Press), 169
- Hjorth, J., Sollerman, J., Møller, P., et al. 2003, *Natur*, **423**, 847
- Ho, A. Y. Q., Phinney, E. S., Ravi, V., et al. 2019, *ApJ*, **871**, 73
- Högbom, J. A. 1974, *A&AS*, **15**, 417
- Hurley, K., Golenetskii, S., Aptekar, R., et al. 2010, in *AIP Conf. Ser. 1279*, *Deciphering the Ancient Universe with Gamma-Ray Bursts*, ed. N. Kawai & S. Nagataki (Melville, NY: AIP), 330
- Hurley, K., Svinkin, D. S., Aptekar, R. L., et al. 2016, *ApJL*, **829**, L12
- Irwin, C. M., & Chevalier, R. A. 2016, *MNRAS*, **460**, 1680
- Japelj, J., Vergani, S. D., Salvaterra, R., et al. 2018, *A&A*, **617**, A105
- Jones, F. C., & Ellison, D. C. 1991, *SSRv*, **58**, 259
- Kasen, D. 2017, in *Handbook of Supernovae*, ed. A. Alsabti & P. Murdin (Cham: Springer), 939
- Kasliwal, M. M., Cannella, C., Bagdasaryan, A., et al. 2019, *PASP*, **131**, 038003
- Kulkarni, S. R., Frail, D. A., Wieringa, M. H., et al. 1998, *Natur*, **395**, 663
- Laskar, T., Coppejans, D. L., Margutti, R., & Alexander, K. D. 2017, *GCN*, **22216**, 1
- Lazzati, D., Morsony, B. J., Blackwell, C. H., et al. 2012, *ApJ*, **750**, 68
- Li, L.-X. 2006, *MNRAS*, **372**, 1357
- Lupton, R., Blanton, M. R., Fekete, G., et al. 2004, *PASP*, **116**, 133
- Lyman, J. D., Bersier, D., James, P. A., et al. 2016, *MNRAS*, **457**, 328
- MacFadyen, A. I., Woosley, S. E., & Heger, A. 2001, *ApJ*, **550**, 410
- Mahabal, A., Rebbapragada, U., Walters, R., et al. 2019, *PASP*, **131**, 038002
- Malesani, D., Tagliaferri, G., Chincarini, G., et al. 2004, *ApJL*, **609**, L5
- Margutti, R., Guidorzi, C., Lazzati, D., et al. 2015, *ApJ*, **805**, 159
- Margutti, R., Milisavljevic, D., Soderberg, A. M., et al. 2014, *ApJ*, **797**, 107
- Margutti, R., Soderberg, A. M., Wieringa, M. H., et al. 2013, *ApJ*, **778**, 18
- Masci, F. J., Laher, R. R., Rusholme, B., et al. 2019, *PASP*, **131**, 018003
- McMullin, J. P., Waters, B., Schiebel, D., Young, W., & Golap, K. 2007, in *ASP Conf. Ser. 376*, *Astronomical Data Analysis Software and Systems XVI*, ed. R. A. Shaw, F. Hill, & D. J. Bell (San Francisco, CA: ASP), 127
- Milisavljevic, D., Margutti, R., Parrent, J. T., et al. 2015, *ApJ*, **799**, 51
- Mirabal, N., Halpern, J. P., An, D., et al. 2006, *ApJL*, **643**, L99
- Modjaz, M., Liu, Y. Q., Bianco, F. B., & Graur, O. 2016, *ApJ*, **832**, 108
- Nakar, E. 2015, *ApJ*, **807**, 172
- Oke, J. B., Cohen, J. G., Carr, M., et al. 1995, *PASP*, **107**, 375
- Oke, J. B., & Gunn, J. E. 1982, *PASP*, **94**, 586
- Patat, F., Cappellaro, E., Danziger, J., et al. 2001, *ApJ*, **555**, 900
- Patterson, M. T., Bellm, E. C., Rusholme, B., et al. 2019, *PASP*, **131**, 018001
- Perley, D. A. 2019, *PASP*, **131**, 084503
- Perley, R. A., Chandler, C. J., Butler, B. J., et al. 2011, *ApJL*, **739**, L1
- Pian, E., Mazzali, P. A., Masetti, N., et al. 2006, *Natur*, **442**, 1011
- Piran, T. 2004, *RvMP*, **76**, 1143
- Planck Collaboration, Ade, P. A. R., Aghanim, N., et al. 2016, *A&A*, **594**, A13
- Preece, R. D., Briggs, M. S., Mallozzi, R. S., et al. 2000, *ApJS*, **126**, 19
- Prentice, S. J., Mazzali, P. A., Pian, E., et al. 2016, *MNRAS*, **458**, 2973
- Rigault, M., Neill, J. D., Blagorodnova, N., et al. 2019, *A&A*, **627**, A115
- Sakamoto, T., Lamb, D. Q., Graziani, C., et al. 2004, *ApJ*, **602**, 875
- Salas, P., Bauer, F. E., Stockdale, C., & Prieto, J. L. 2013, *MNRAS*, **428**, 1207
- Sobacchi, E., Granot, J., Bromberg, O., & Sormani, M. C. 2017, *MNRAS*, **472**, 616
- Soderberg, A. M., Chakraborti, S., Pignata, G., et al. 2010, *Natur*, **463**, 513
- Soderberg, A. M., Kulkarni, S. R., Berger, E., et al. 2004a, *ApJ*, **606**, 994
- Soderberg, A. M., Kulkarni, S. R., Berger, E., et al. 2004b, *Natur*, **430**, 648
- Soderberg, A. M., Kulkarni, S. R., Berger, E., et al. 2005, *ApJ*, **621**, 908
- Soderberg, A. M., Kulkarni, S. R., Nakar, E., et al. 2006, *Natur*, **442**, 1014
- Stanek, K. Z., Matheson, T., Garnavich, P. M., et al. 2003, *ApJL*, **591**, L17
- Starling, R. L. C., Wiersema, K., Levan, A. J., et al. 2011, *MNRAS*, **411**, 2792
- Sutherland, P. G., & Wheeler, J. C. 1984, *ApJ*, **280**, 282
- Tachibana, Y., & Miller, A. A. 2018, *PASP*, **130**, 128001
- Taddia, F., Sollerman, J., Fremming, C., et al. 2019, *A&A*, **621**, A71
- Thomsen, B., Hjorth, J., Watson, D., et al. 2004, *A&A*, **419**, L21
- Valenti, S., Benetti, S., Cappellaro, E., et al. 2008, *MNRAS*, **383**, 1485
- Wang, J., Zhu, Z. P., Xu, D., et al. 2018, *ApJ*, **867**, 147
- Watson, D., Hjorth, J., Levan, A., et al. 2004, *ApJL*, **605**, L101
- Woosley, S., & Janka, T. 2005, *NatPh*, **1**, 147
- Woosley, S. E., & Bloom, J. S. 2006, *ARA&A*, **44**, 507
- Woosley, S. E., Eastman, R. G., & Schmidt, B. P. 1999, *ApJ*, **516**, 788
- Yao, Y., Miller, A. A., Kulkarni, S. R., et al. 2019, *ApJ*, **886**, 152
- Yaron, O., & Gal-Yam, A. 2012, *PASP*, **124**, 668
- Zackay, B., Ofek, E. O., & Gal-Yam, A. 2016, *ApJ*, **830**, 27